# Nonlinear Throttle Control

Paul Griffiths

May 8, 2001

## 1 Introduction

In this control design project, adaptive sliding surface control is applied to control of engine throttle angle. This application of adaptive sliding surface control could be useful in drive-by-wire systems, in which the direct linkages between the accelerator and the throttle or the steering wheel and the the steering gear are replaced with pairs of sensors and actuators. Currently, drive-by-wire systems exist primarily in heavy-duty equipment like earth moving or farming equipment. For these systems to be install on passenger vehicles, they must be shown to have equivalent safety and reliability compared with the mechanical linkage, and offer some benefit that justifies the additional cost.

The nonlinear control design presented in this paper has robust performance with respect to uncertainty of plant parameters. In addition, an adaption law for an estimate of the Coulumb friction in the throttle body guarantees that the estimate converges to the real plant value. The controller uses the friction estimate to apply only the necessary actuation torque to the throttle plate. In this way, the controller uses less power and it can alert the driver when the friction in the throttle body is abnormally large.

## 2 Throttle Body

The particular throttle body, for which the controllers are designed, is test set-up mounted to a thick steel base. Off one side of the throttle body is a potentiometer, which measures the angle of the throttle plate. Off the other side is a DC motor and return spring. Figure 1 shows a simplified diagram of the throttle body steup. Table 1 identifies the parameters that are used in the equations of motion for the system.

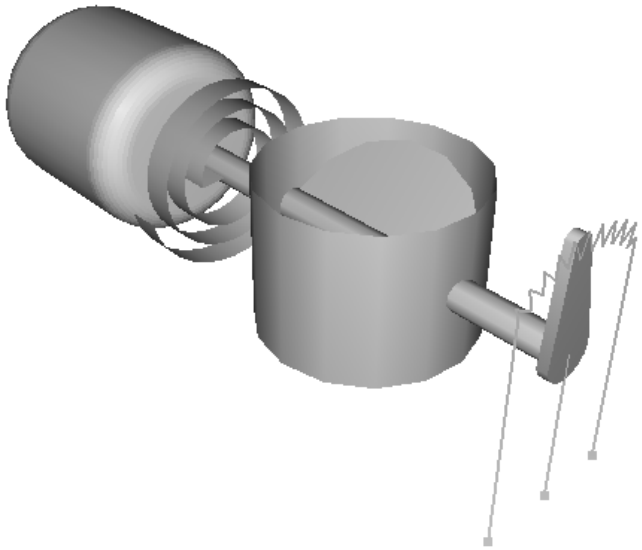

Figure 1: Diagram of throttle body with DC motor, throttle position sensor and return spring

Table 1: Plant Parameters

| Parameter | Estimated Value | Units | Description |
|---|---|---|---|
| $J$ | 5.0e-4 | $kg \cdot m^2$ | Equivalent moment of inertia |
| $K_s$ | 0.020 | $\frac{N \cdot m}{rad}$ | Torsional spring constant |
| $K_f$ | 0.0070 | $N \cdot m$ | Coulumb friction |
| $K_d$ | 0.0050 | $\frac{N \cdot m}{rad \cdot s}$ | Viscous damping |
| $R_a$ | 1.70 | $\Omega$ | Armeture Resistance |
| $L_a$ | 0 | $H$ | Armeture Inductance |
| $K_T$ | 0.012 | $\frac{N \cdot m}{A}$ | Proportionality Constant |
| $\theta_{eq}$ | -0.25 | $rad$ | Equilibrium Angle |

# 3 Throttle Body Equations of Motion

The Kirchoff loop equation for the armeture circuit is given by equation 1

$$R_a i_a + L_a \frac{di_a}{dt} + V_b(t) = e_a(t) \quad (1)$$

$$V_b(t) = K_T \frac{d\theta_m}{dt} \quad (2)$$

$$i_a(t) = \frac{1}{K_T} T_m(t) \quad (3)$$

Equation 2 gives the back EMF in the armeture circuit as a function of motor speed. The current through the circuit is given by equation 3 and is a derivation of a power equation, which equates the power into the armeture circuit with the mechanical power done by the motor. Substituting equation 2 and 3 into 1 gives,

$$\frac{R_a T_m(t)}{K_T} + \frac{L_a}{K_T} \dot{T_m} + K_T \dot{\theta} = e_a(t) \quad (4)$$

The torque $T_m(t)$ can be expressed as the mechanical load on the motor.

$$T_m(t) = J_m \ddot{\theta} + K_d \dot{\theta} + K_f sgn(\dot{\theta}) + K_s(\theta - \theta_e q) \quad (5)$$

The $sgn(\dot{\theta})$ makes it impossible to find $\dot{T_m}$, but if $L_a$ is assumed to be zero, then $\dot{T_m}(t)$ does not need to be calculated. Using this assumption about $L_a$, the final set of differential equations are,

$$\dot{\theta} = \omega \quad (6)$$

$$\dot{\omega} = \left(-\frac{K_T^2}{R_a J_m} - \frac{K_d}{J_m}\right)\omega - \left(\frac{K_f}{J_m}\right) sgn(\omega) - \left(\frac{K_s K_T}{R_a J_m}\right)(\theta - \theta_{eq}) \quad (7)$$

$$+ \left(\frac{K_T}{R_a J_m}\right) e_a \quad (8)$$

# 4 System Identification

The parameters have been selected to match the step response of the actual throttle as closely as possible. The step response is shown in figure 2. The throttle angle is measured as milli-Volts, which can be mapped to the range of angles, 0 to $\frac{\pi}{2}$. The plot shows the thottle angle rise after full power (10 Volts) was applied the motor and then, after the power was turned off, the

throttle closed under the influence of the return spring. The first portion of the plot is useful in determining the motor parameters, but it requires knowledge of the effect of the return spring. The second portion of the plot shows the effect of the return spring and friction. These two effects can be separated because the return spring is linear with position, whereas friction is a function of velocity.

An iterative approach is necessary to find the parameters $\frac{K_s}{J}$, $\frac{K_d}{J}$ and $\frac{K_f}{J}$. These parameters were fit in a least squares sense to the step response data of the throttle dropping from wide open to closed. This data is in graph 4. An initial value for $\frac{K_s}{J}$ is found without compensating for the effect of friction. Then $\frac{K_d}{J}$ and $\frac{K_f}{J}$ are found including the effect of $\frac{K_s}{J}$. This process quickly yields estimates of the parameters, given in table 2.

Table 2: Estimated System Parameters for Step Response

| Parameter | Estimated Value | Units |
|---|---|---|
| $\frac{K_s}{J}$ | 390 | $\frac{1}{s^2}$ |
| $\frac{K_d}{J}$ | -0.87 | $\frac{1}{s}$ |
| $\frac{K_f}{J}$ | 140 | $\frac{rad}{s^2}$ |

The viscous damping coefficient, $K_d$, is negative but should be positive. It appears that the absolute value of the damping is small compared with the noise in the measurements. In order to make the plant model dissipate energy rather than gain energy through friction, $\frac{K_f}{J}$ is set to 1.0. This factor has a small effect when compared with the effect of the spring and Coulumb friction.

During the throttle step response from closed to wide open, the angular acceleration is nearly constant. This is shown in graph 3. The typical response of DC motors is that the angular acceleration decreases as the angular velocity increases. The back-EMF accounts for this effect in the system equations, and the constant angular acceleration over the values of angular velocity in the step response indicate the following approximations.

$$\frac{K_T}{R_a J} \approx 1400 \left(\frac{rad}{s^2}\right) \tag{9}$$

$$\frac{K_T^2}{R_a J}\omega \approx 0 \tag{10}$$

The resistance of the armeture of the motor was measured to be 1.7$\Omega$, so only the mass moment of inertia of the motor remains to be estimated to

calculate the values of $K_s$, $K_d$, $K_f$ and $K_T$. This parameter was estimated based on some rough assumptions on the geometry of the motor rotor and throttle as well as assuming that the parts were made out of steel. This estimated inertia must also be small such that $K_T \gg K_T^2\omega$, for $|\omega|$ up to $50(\frac{rad}{s})$.

The plant model created is used to test the adaptive sliding surface controllers. For controllers that use knowledge of parameter uncertainty, the parameters, $K_s, K_d, K_f, K_T, J$ and $R_a$, are eached assumed to vary as much as $\pm 2\%$ from their nominal values. This value was selected arbitrarily for the sake of demonstrating the controllers. If these controllers were to be applied to a production throttle, the manufacturing specifications for the motor and the throttle body would be provide bounds on the plant parameters.

# 5 Sliding Surface Control

A Lyanpunov function V is defined in equation 11 and 12. If $\dot{V}$ is made negative definite, then s will globally, asymtotically approach zero. Then $s$ is designed so that $s = 0$ makes the plant states approach the desired values. Equation 13 defines $s$, the sliding surface, and clearly, for positive values of $\lambda$, $\theta$ will linearly decay towards $\theta_d$.

$$V = \frac{1}{2}s^2 \tag{11}$$

$$\dot{V} = s\dot{s} \tag{12}$$

$$s = (\omega - \omega_d) + \lambda(\theta - \theta_d) \tag{13}$$

$$\begin{aligned} \dot{s} = & \left(-\frac{K_T^2}{R_a J_m} - \frac{K_d}{J_m}\right)\omega - \left(\frac{K_f}{J_m}\right) sgn(\omega) \\ & - \left(\frac{K_s K_T}{R_a J_m}\right)(\theta - \theta_{eq}) + \left(\frac{K_T}{R_a J_m}\right) e_a - \omega_d + \lambda\,(\theta - \theta_d) \end{aligned} \tag{14}$$

Equation 13 is also a good choice for $s$, because the input, $e_a$, shows up in $\dot{s}$. An appropriate sliding surface control law drives $e_a$ in such a way that $s\dot{s}$ is negative definite.

## 5.1 Sliding Surface without Uncertainty

If the plant parameters are known exactly, then making $\dot{s}$ zero is simply a matter of canceling the plant dynamics. Equation 15 gives the control, $e_a$. An additional term, $-\eta sgn(s)$ forces $s\dot{s}$ to be negative definite.

$$e_a = \Big[(K_T + \frac{R_a K_d}{K_T})\omega + \frac{R_a K_f}{K_T} sgn(\omega) \frac{R_a K_s}{K_T}(\theta - \theta_{eq}) + \frac{R_a J}{K_T}(\dot{\omega_d} - \lambda(\omega - \omega_d))\Big] - \eta sgn(s) \quad (15)$$

Figure 5 shows $\theta$, $\theta_d$, $\omega$ and $e_a$ for a simulation of this controller. The sliding surface control parameters were set as follows: $\eta = 1.5(V)$ and $\lambda = 30$. Runga-Kutta 2/3 with variable step size was used to solve the simulation ode's; a maximum step size of 2 milliseconds was specified to keep the desired angle smooth. The throttle is initially closed, and within about 0.15 seconds the sliding surface is reached. The throttle angle is brought within about 2% of the desired value in approximately 0.25 seconds. The desired throttle angle cycles between wide open and closed with a period of 1 second and the actual angle tracks the desired value very closely.

## 5.2 Sliding Surface with Uncertainty

When the nominal value of plant parameters and the absolute error of the plant parameters are known, equation 15 must have some additional terms appended to it to ensure that $s\dot{s}$ is negative definite. The error in each term of the original control law is upper bounded by the following,

$$C1 = |K_{T_{max}} - K_{T_{min}}| \quad (16)$$

$$C2 = \left| \frac{R_{a_{max}} K_{d_{max}}}{K_{T_{min}}} - \frac{R_{a_{min}} K_{d_{min}}}{K_{T_{max}}} \right| \quad (17)$$

$$C3 = \left| \frac{R_{a_{max}} K_{f_{max}}}{K_{T_{min}}} - \frac{R_{a_{min}} K_{f_{min}}}{K_{T_{max}}} \right| \quad (18)$$

$$C4 = \left| \frac{R_{a_{max}} K_{s_{max}}}{K_{T_{min}}} - \frac{R_{a_{min}} K_{s_{min}}}{K_{T_{max}}} \right| \quad (19)$$

$$C5 = \left| \frac{R_{a_{max}} J_{max}}{K_{T_{min}}} - \frac{R_{a_{min}} J_{min}}{K_{T_{max}}} \right| \quad (20)$$

The maximum and minimum values for $\hat{R_a}$, $\hat{K_d}$, $\hat{K_f}$, $\hat{K_s}$ and $\hat{J}$ are easily calculated based on the uncertainty of $\pm 2\%$ in each parameter. The upper bound on the error of each term in the original equation for $e_a$ (eqn. 15) can be used to develop the new expression for $e_a$,

$$
\begin{aligned}
e_a \;=\; & \left[\left(\hat{K_T} + \frac{\hat{R_a}\hat{K_d}}{\hat{K_T}}\right)\omega + \frac{\hat{R_a}\hat{K_f}}{\hat{K_T}} sgn(\omega) + \frac{\hat{R_a}\hat{K_s}}{\hat{K_T}}(\theta - \theta_{eq}) \right. \\
& \left. + \frac{\hat{R_a}\hat{J}}{\hat{K_T}}(\dot{\omega_d} - \lambda(\omega - \omega_d))\right] \\
& - \left[(C1 + C2)|\omega| + C3 + C4|\theta - \theta_{eq}| \right. \\
& \left. + C5|\dot{\omega_d} - \lambda(\omega - \omega_d)| + \eta\right] sgn(s)
\end{aligned} \tag{21}
$$

Figure 6 shows $\theta$, $\theta_d$, $\omega$ and $e_a$ for a simulation of this controller. The sliding surface control parameters and the solver settings were the same as those used in the simulation of the sliding surface control without uncertainty. The plant's value of $K_s$ was increased by 2% and the value of $K_T$ decreased by 2%. There are two features to be noted in the simulation results; the tracking is nearly identical to the simple sliding surface controller and the control input is larger for the controller that is compensating for the parameter uncertainty. In general, the sliding surface controller maintains the same performance under increasing uncertainty only at the cost of higher control effort.

# 6 Adaptive Sliding Surface Control

It would be nice to have an estimate of the Coulumb friction, $K_f$. With an estimate of this value, the control input could be reduced because it would not have to handle the worst case friction. If the estimate shows that the friction is abnormally high (compared with some design specification for the throttle body), a diagnositic message could be displayed.

The Lyapunov function defined in equation 11 is altered to include a parameter estimation error term,

$$\tilde{K_f} = \hat{K_f} - K_f \tag{22}$$

$$V = \frac{1}{2}s^2 + \frac{1}{2\gamma}\tilde{K_f}^2 \tag{23}$$

$$\dot{V} = s\dot{s} + \frac{1}{\gamma}\tilde{K_f}\dot{\tilde{K}}_f \tag{24}$$

## 6.1 Adaptive Sliding Surface without Uncertainty

Because $\hat{K_f}$ in equation 24 is not an uncertainty nor is it equal to the actual plant value, the control, $e_a$, cannot cancel it out. Using the original sliding

surface control without considering uncertainty, $\dot{V}$ becomes,

$$\dot{V} = -\eta s sgn(s) + \frac{1}{J}\tilde{K_f} sgn(\omega) s + \frac{1}{\gamma}\tilde{K_f}\dot{\hat{K}_f} \tag{25}$$

The first term, $-\eta s sgn(s)$, is already negative, so the adaption law for $\hat{K_f}$ must be chosen to make the remaining terms negative definite.

$$\frac{1}{J}\tilde{K_f} sgn(\omega) s + \frac{1}{\gamma}\tilde{K_f}\dot{\hat{K}_f} \leq 0 \tag{26}$$

$$\dot{K_f} = 0 \tag{27}$$

$$\tilde{K_f}\left(\frac{1}{J} sgn(\omega) s + \frac{1}{\gamma}\dot{\hat{K}_f}\right) \leq 0 \tag{28}$$

$$\frac{1}{J} sgn(\omega) s + \frac{1}{\gamma}\dot{\hat{K}_f} = 0 \tag{29}$$

$$\dot{\hat{K}_f} = -\frac{\gamma}{J} sgn(\omega) s \tag{30}$$

Equation 30 is an adaption law that makes $\dot{V}$ the same as it was in the original sliding surface control by cancelling ou the terms with $\tilde{K_f}$. There is a substantial difference though between the Lyapunov functions. In the new Lyapunov function there is no guarentee on the initial convergence of $\hat{K_f}$ towards $K_f$ (if $s \neq 0$). It is only after $s \approx 0$ that the convergence of $\tilde{K_f} \rightarrow 0$ is strictly enforced by the definition of $V$ and $\dot{V}$.

Figure 7 shows $\theta$, $\theta_d$, $\omega$ and $e_a$ for a simulation of this adaptive controller. Figure 8 shows $\hat{K_f}$ and $\dot{\hat{K}_f}$. The adaption parameter, $\gamma$, was set to $1e-6$ and the same sliding surface control and simulation setup were used as in the sliding surface control simulation. The simulation results show that the controller has some over-shoot that was not present with the sliding mode controllers. This over-shoot causes the actual throttle angle to settle to the desired angle about 0.05 seconds later. The adaption of $\hat{K_f}$, after some initial floating around, converges within 5% of the actual value of $K_f$ in slightly less than 2 seconds.

## 6.2 Adaptive Sliding Surface with Uncertainty

Extending the adaptive sliding surface control to compensate for parameter uncertainty does not require much modification to the work already done. $K_f$ must be brought out of $C3$, which changes $C3$ and $e_a$.

$$C3 = \left| \frac{R_{a_{max}}}{K_{T_{min}}} - \frac{R_{a_{min}}}{K_{T_{max}}} \right| \tag{31}$$

$$\begin{aligned} e_a = & \left[ \left( \hat{K_T} + \frac{\hat{R_a}\hat{K_d}}{\hat{K_T}} \right) \omega + \frac{\hat{R_a}\hat{K_f}}{\hat{K_T}} sgn(\omega) + \frac{\hat{R_a}\hat{K_s}}{\hat{K_T}} (\theta - \theta_{eq}) \right. \\ & \left. + \frac{\hat{R_a}\hat{J}}{\hat{K_T}} (\dot{\omega_d} - \lambda(\omega - \omega_d)) \right] \\ & - \left[ (C1 + C2)|\omega| + C3|\hat{K_f}| + C4|\theta - \theta_{eq}| \right. \\ & \left. + C5|\dot{\omega_d} - \lambda(\omega - \omega_d)| + \eta \right] sgn(s) \end{aligned} \tag{32}$$

The Lyapunov function must be examined again because $\frac{\hat{K_f}}{J}$ has become $\frac{K_T}{R_a J} \left( \frac{\hat{R_a}\hat{K_f}}{\hat{K_T}} sgn(\omega) \right)$. It turns out though that the uncertainty accounted for by $C3$ makes sure that the new expression is always less than or equal to the original.

$$\frac{K_T}{R_a J} \left( \frac{\hat{R_a}\hat{K_f}}{\hat{K_T}} sgn(\omega) \right) - \frac{K_T}{R_a J} C3|\hat{K_f}| \leq \frac{\hat{K_f}}{J} \tag{33}$$

This result means that $\dot{V}$ is at least as negative as it was originally. Therefore, the same adaption law will work. Figure 9 plots $\theta$, $\theta_d$, $\omega$ and $e_a$ versus time for a simulation of this adaptive controller. Figure 10 plots $\hat{K_f}$ and $\dot{\hat{K}}_f$ versus time. All of the parameters from the sliding mode design and the adaptive design were used in the combined simulation. The simulation had to be run twice as long as the first adaptive design to see the same convergence of $\hat{K_f}$ to $K_f$ and the control input is larger than in the first design.

# 7 Conclusions

The adaptive sliding surface controller is able to identify the static friction in the throttle body. This could be used as a diagnostic measure. For instance, if the estimated friction parameter were to exceed twice the nominal value, a warning light could be turned on. The warning light would indicate the possible poor performance or failure of the control system due to excessive friction and the need to clean or replace the throttle body.

Besides being a good diagnostic tool, the adaptive sliding surface controller will save power compared with a non-adaptive sliding surface controller. A simulation was set up to calculate the difference in power con-

sumption using the two different controllers. The energy into the motor was calculated by $\frac{1}{R_a}\int_{t_1}^{t_2} e_a^2 d\tau$, and this integral over one second gives an approximate power usage in Watts. The estimate is actually very accurate since the desired throttle angle, which the controller tracks, has a period of 1 second. The scenario selected set $K_f = 0.001$ while all other parameters had $\pm 2\%$ uncertainty, except for $K_f$, which is nominally 0.007, but could range from 0 to 0.014. The desired throttle angle traces a sign wave with a period of 1 second and amplitude of $\frac{\pi}{2}$. The adaptive controller uses 8.3 Watts to track the input, whereas the sliding mode control uses 11.0 Watts. The 32% increase in power required is power wasted on uncertainty that the controller can quantify itself.

# 8 Simulation Results

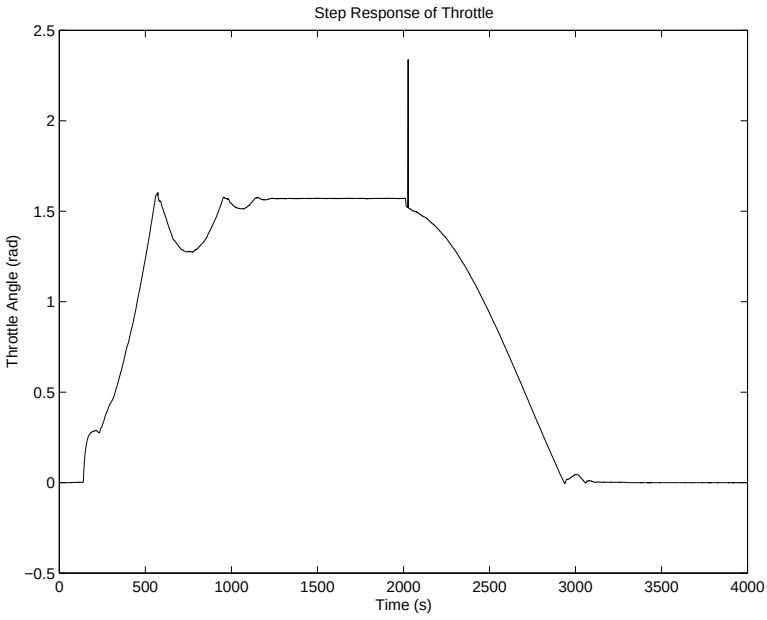


Figure 2: Throttle step response

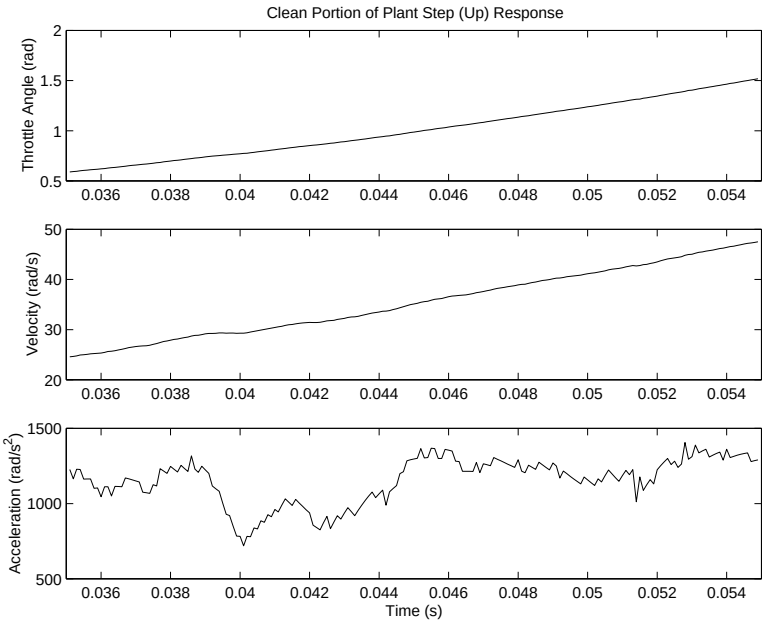


Figure 3: Step response from closed to full open throttle

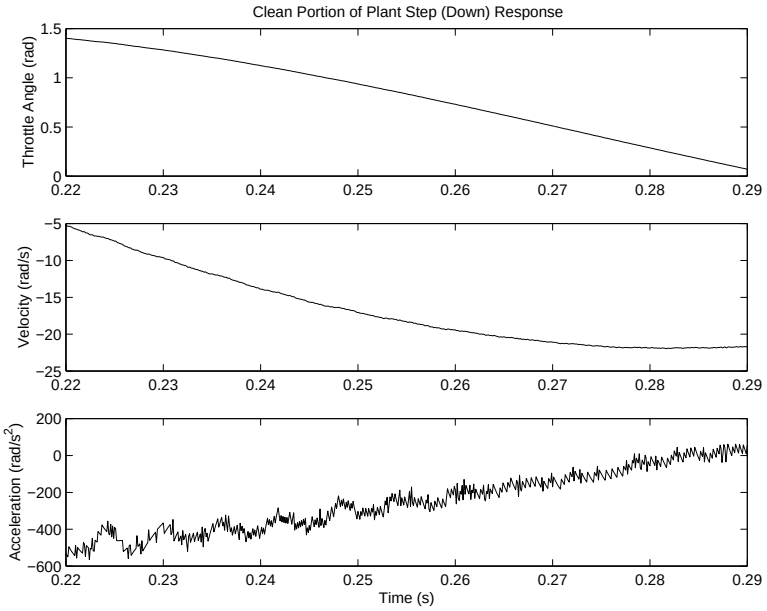


Figure 4: Step response from full optn to closed throttle

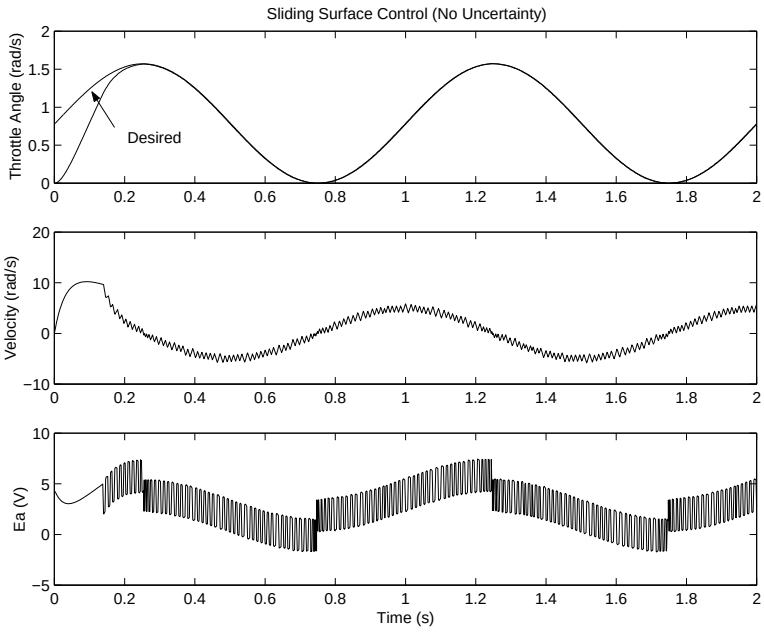


Figure 5: Sliding surface control without parameter uncertainty

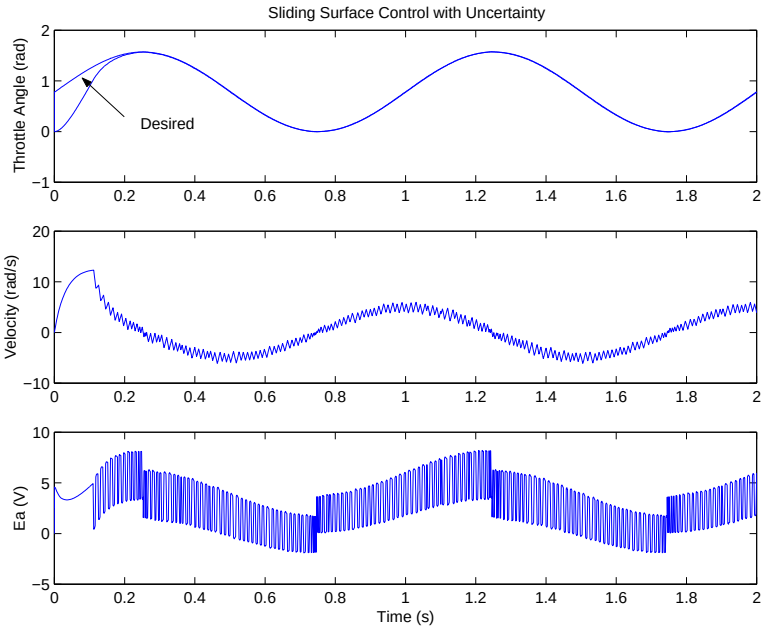


Figure 6: Sliding surface control with +/-2% uncertainty in $K_f, K_s, K_T, K_d, R_a, J$

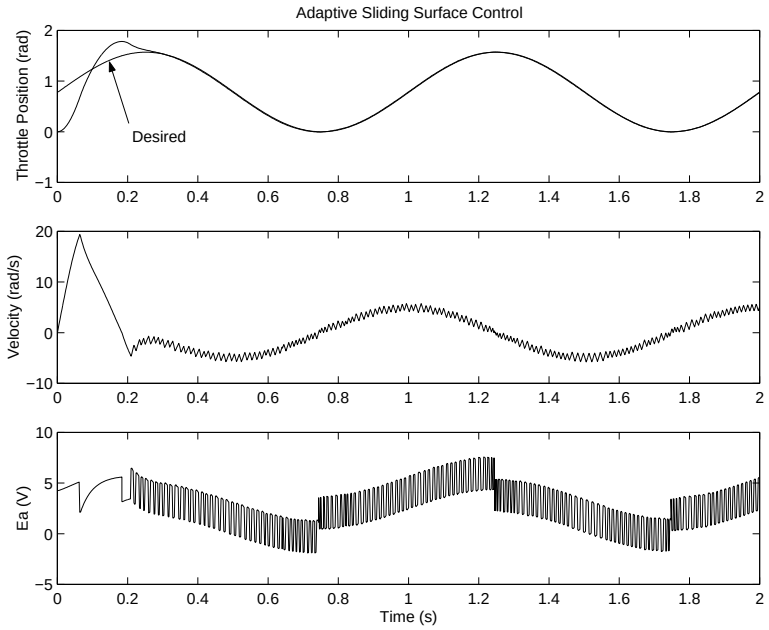


Figure 7: Adaptive sliding surface control without parameter uncertainty

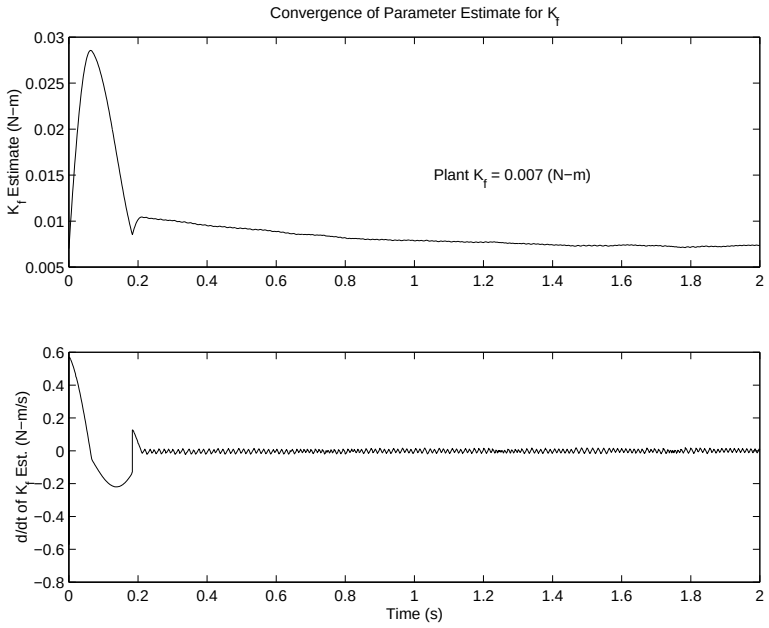


Figure 8: Parameter convergence of $\hat{K_f}$ without parameter uncertainty

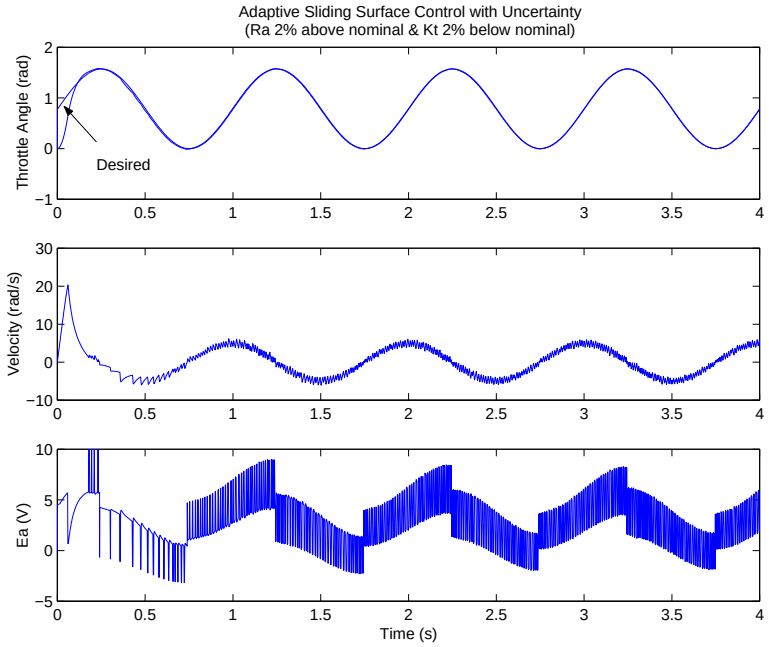


Figure 9: Adaptive sliding surface control with +/-2% uncertainty in $K_f, K_s, K_T, K_d, R_a, J$

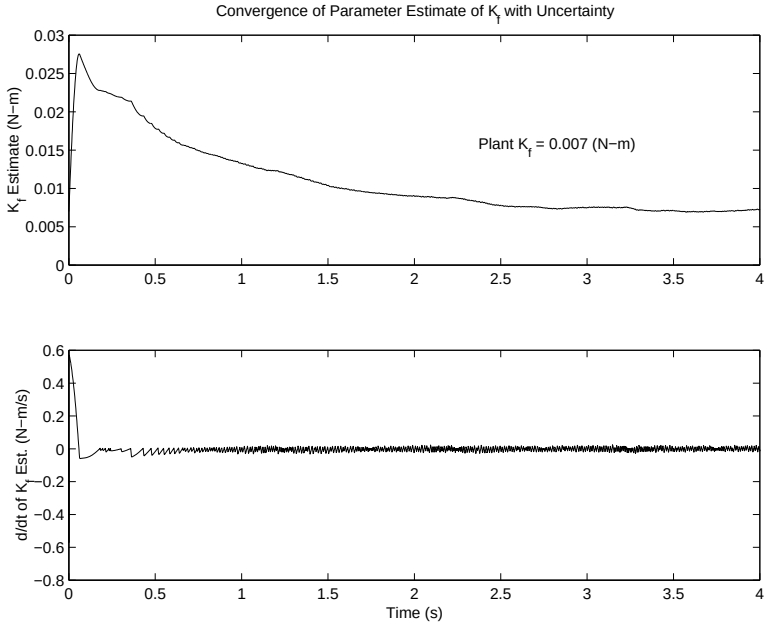


Figure 10: Parameter convergence of $\hat{K_f}$ with parameter uncertainty